US 20200065948A1

(19) **United States**

(12) **Patent Application Publication** (10) **Pub. No.: US 2020/0065948 A1**

Nosher et al. (43) **Pub. Date: Feb. 27, 2020**

(54) **COMPUTATIONAL ULTRASOUND FOR IMPROVED LIVER AND KIDNEY CANCER DIAGNOSIS**

(71) Applicant: **Rutgers, The State University of New Jersey**, New Brunswick, NJ (US)

(72) Inventors: **John Nosher**, Basking Ridge, NJ (US); **Ilker Hacihaliloglu**, Jersey City, NJ (US)

(21) Appl. No.: **16/489,151**

(22) PCT Filed: **Feb. 27, 2018**

(86) PCT No.: **PCT/US18/19945**

§ 371 (c)(1),
(2) Date: **Aug. 27, 2019**

Related U.S. Application Data

(60) Provisional application No. 62/464,058, filed on Feb. 27, 2017.

Publication Classification

(51) **Int. Cl.**

G06T 5/00	(2006.01)
G06T 5/10	(2006.01)
G06T 5/20	(2006.01)
A61B 8/08	(2006.01)

(52) **U.S. Cl.**

CPC ***G06T 5/008*** (2013.01); ***G06T 5/10*** (2013.01); *G06T 2207/30056* (2013.01); ***A61B 8/5207*** (2013.01); *G06T 2207/10132* (2013.01); ***G06T 5/20*** (2013.01)

(57) **ABSTRACT**

This disclosure provides a system and method for generating an ultrasound image. The method includes receiving a raw ultrasound signal output from an ultrasound device and performing operations to transform the raw ultrasound signal into an enhanced ultrasound image. The enhanced ultrasound image may be further processed by radial symmetry filtering to generate a radial symmetry image. Both the enhanced image and the radial symmetry image can be by a medical practitioner to make a liver or kidney cancer diagnosis exclusively based on ultrasound data.

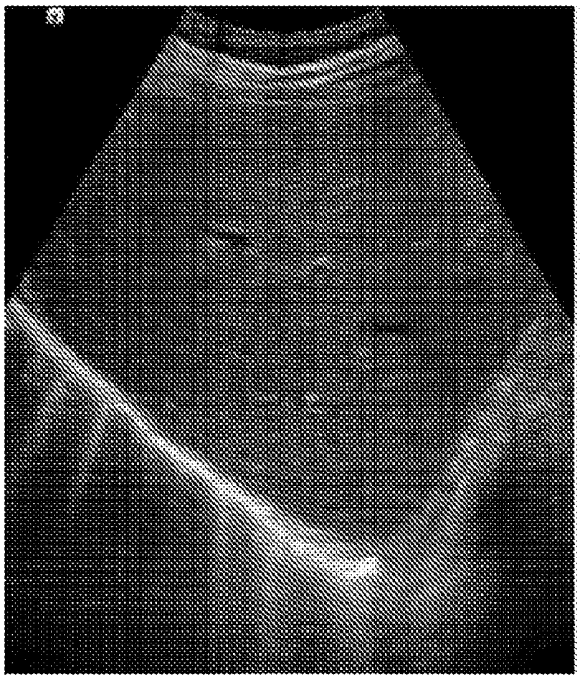

Normal/Healthy Liver

Enhanced Normal/Healthy Liver

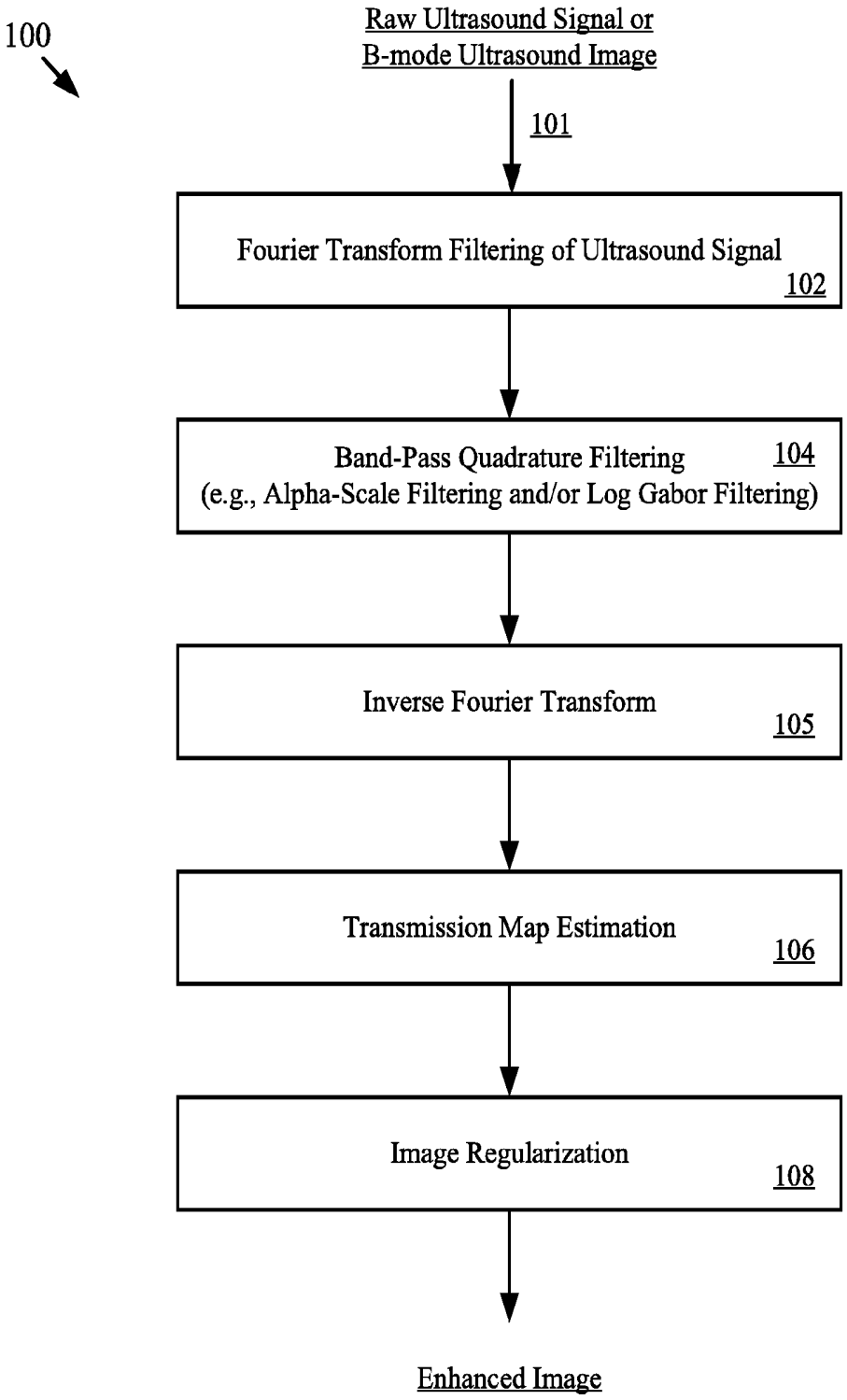
100
Raw Ultrasound Signal or
B-mode Ultrasound Image
101
Fourier Transform Filtering of Ultrasound Signal
102
Band-Pass Quadrature Filtering
(e.g., Alpha-Scale Filtering and/or Log Gabor Filtering)
104
Inverse Fourier Transform
105
Transmission Map Estimation
106
Image Regularization
108
Enhanced Image

FIG. 1

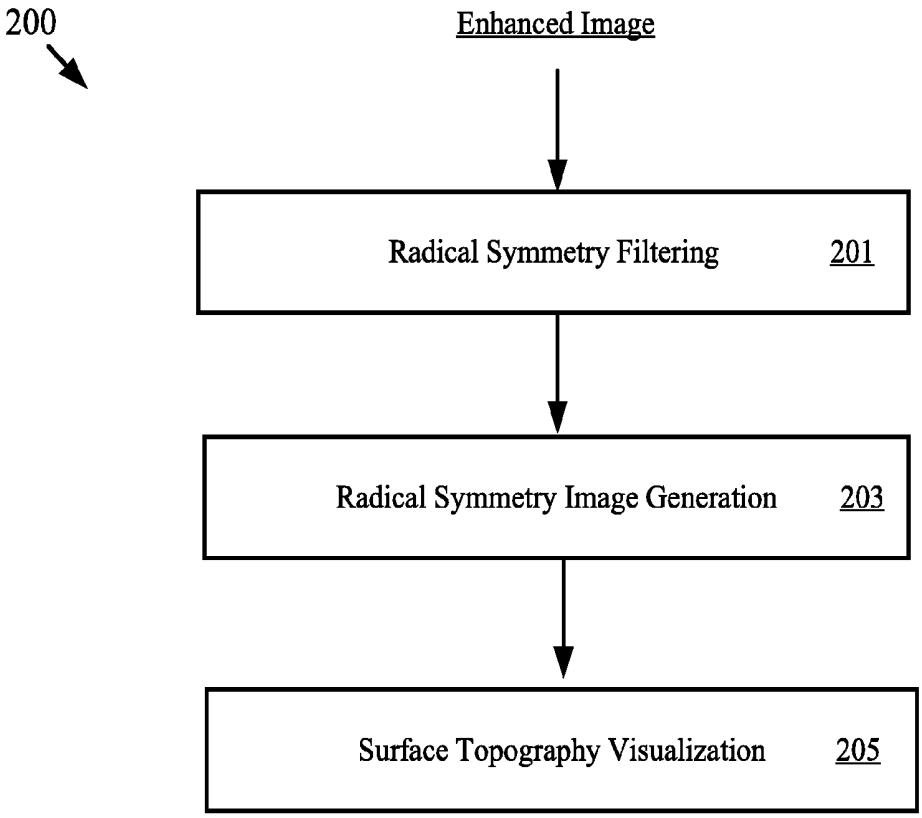
200
Enhanced Image
Radical Symmetry Filtering 201
Radical Symmetry Image Generation 203
Surface Topography Visualization 205

FIG. 2

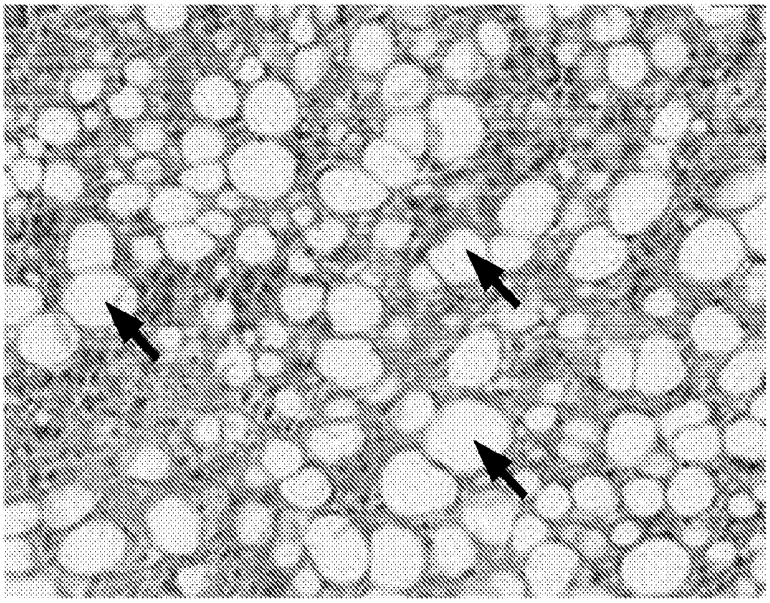

FIG. 3

FIG. 4A

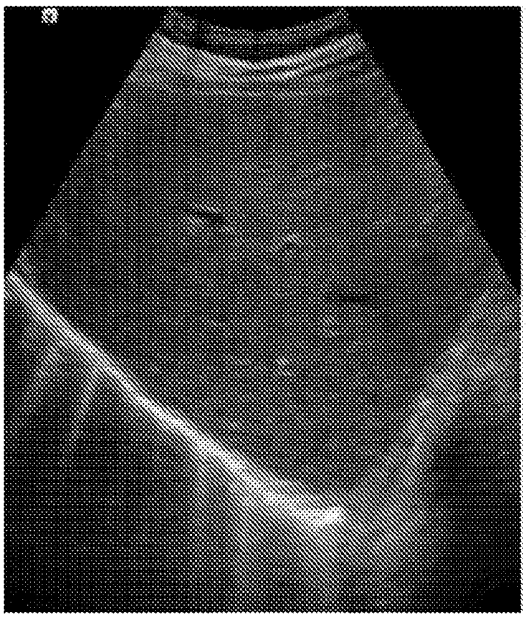

Normal/Healthy Liver

FIG. 4B

Enhanced Normal/Healthy Liver

FIG. 4C

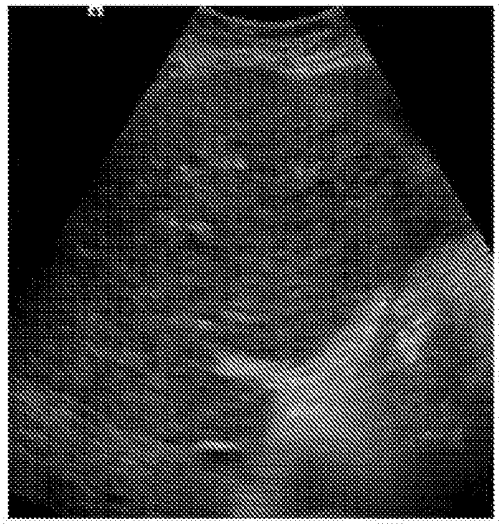

Diseased Liver

FIG. 4D

Enhanced Diseased Liver

FIG. 5A

FIG. 5B

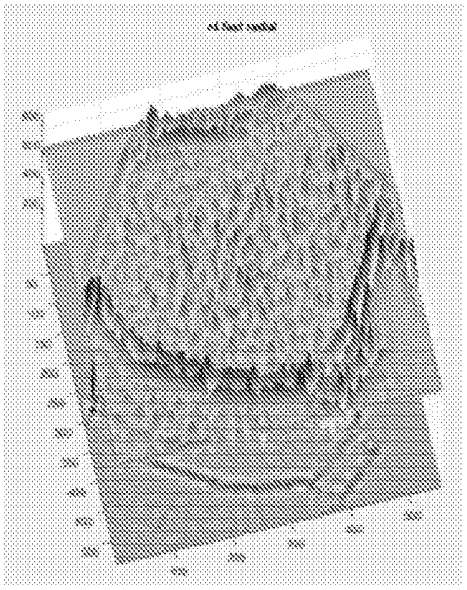

FIG. 5C

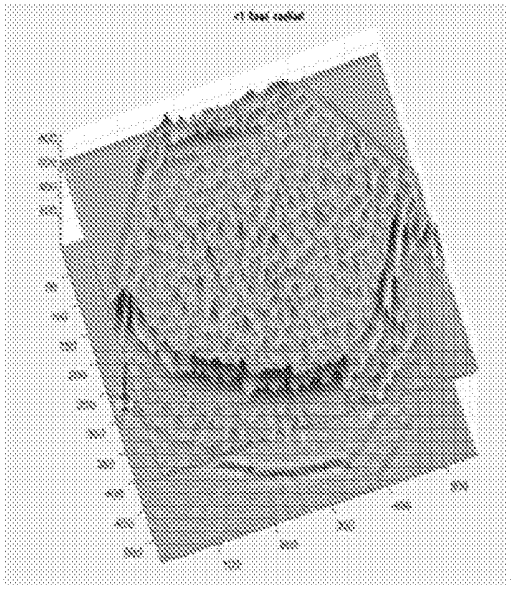

FIG. 5D

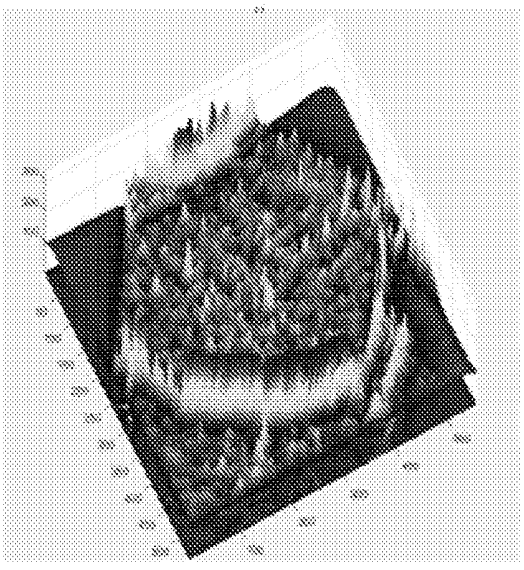

FIG. 5E

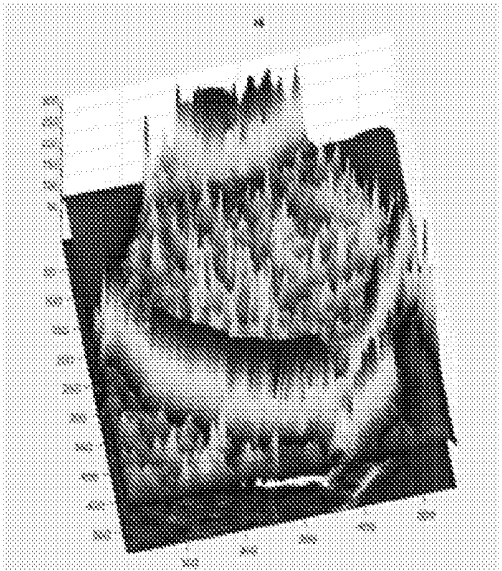

FIG. 6A

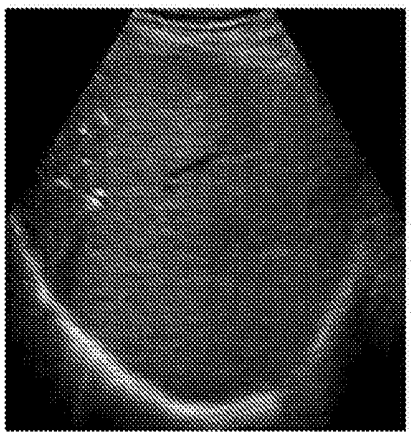

FIG. 6B

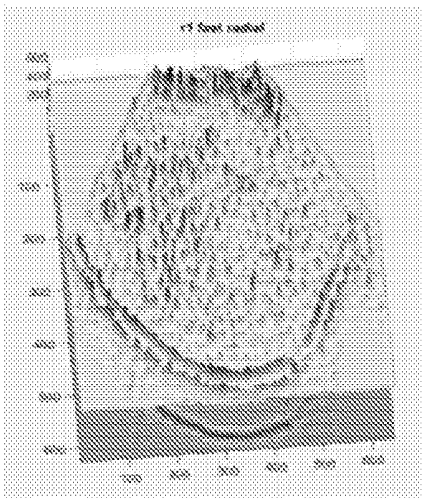

FIG. 6C

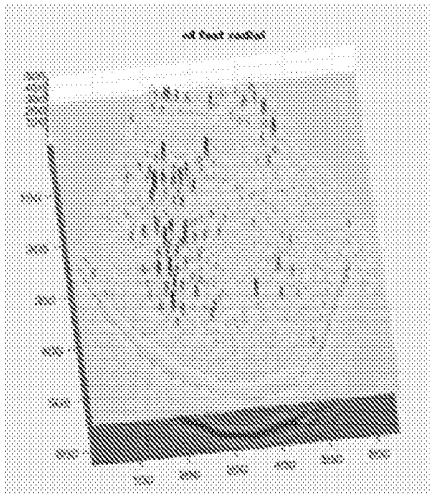

FIG. 6D

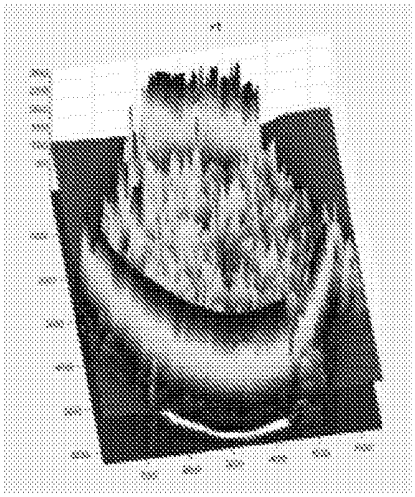

FIG. 6E

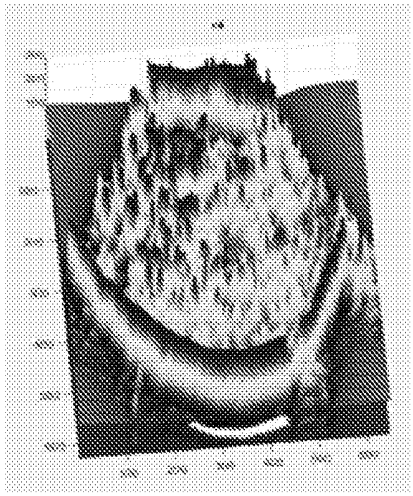

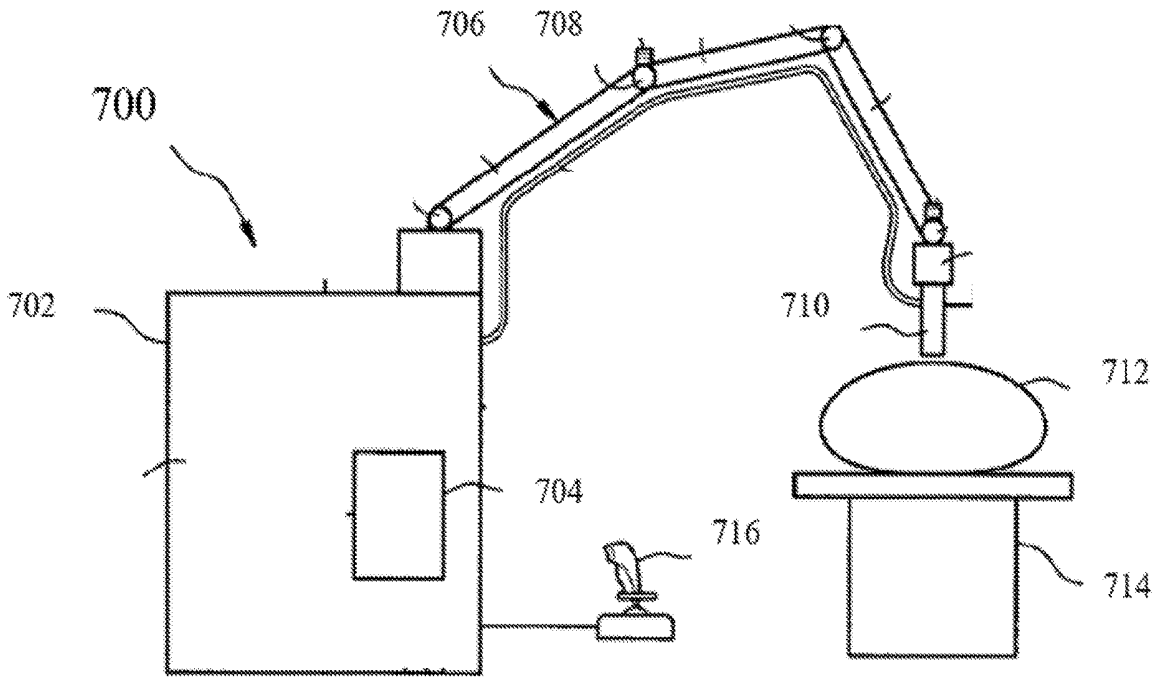

FIG. 7

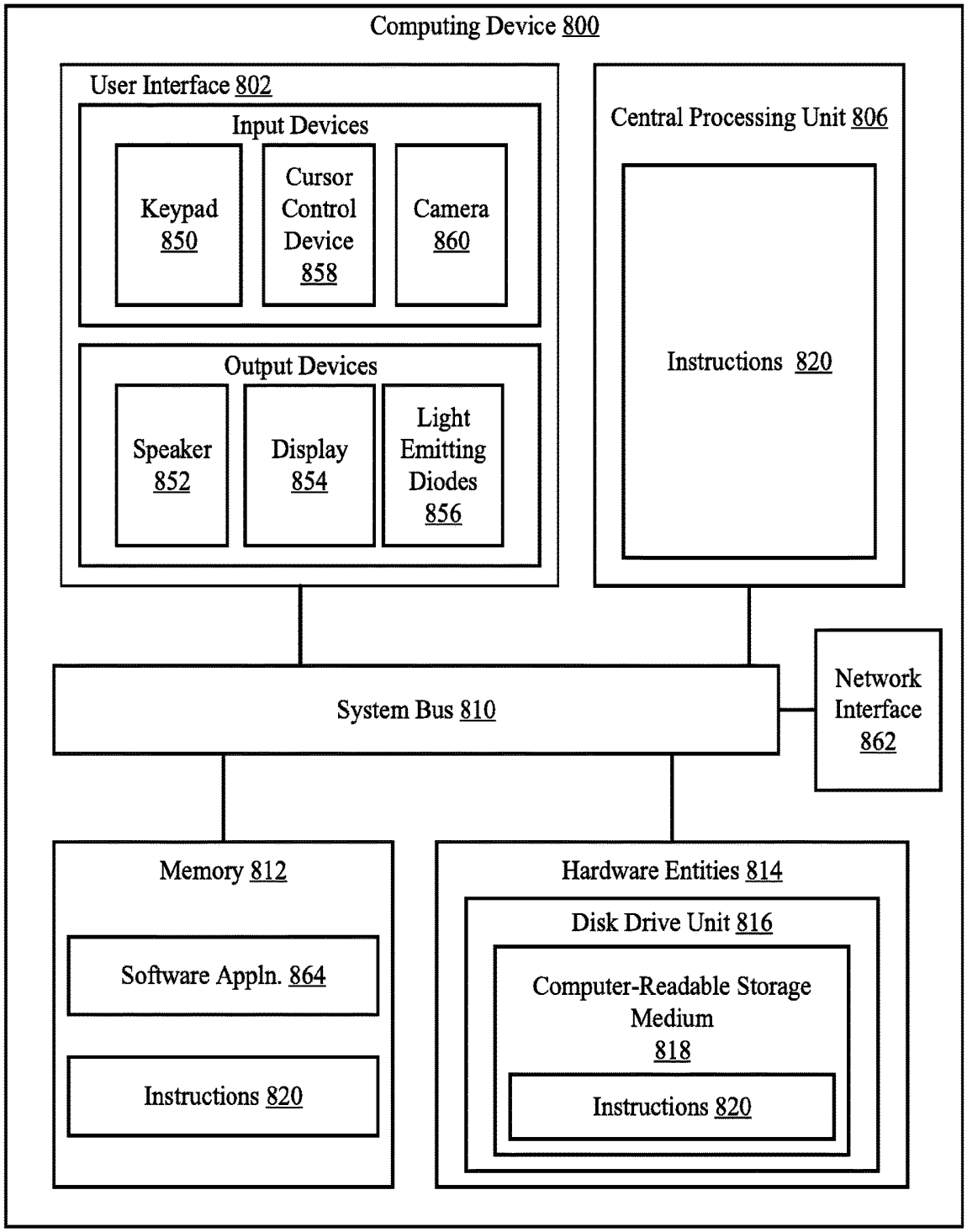
Computing Device 800
User Interface 802
Input Devices
Keypad 850
Cursor Control Device 858
Camera 860
Output Devices
Speaker 852
Display 854
Light Emitting Diodes 856
Central Processing Unit 806
Instructions 820
System Bus 810
Network Interface 862
Memory 812
Software Appln. 864
Instructions 820
Hardware Entities 814
Disk Drive Unit 816
Computer-Readable Storage Medium 818
Instructions 820

FIG. 8

COMPUTATIONAL ULTRASOUND FOR IMPROVED LIVER AND KIDNEY CANCER DIAGNOSIS

CROSS-REFERENCE TO RELATED APPLICATIONS

[0001] This application claims priority under 35 U.S.C. § 119(e) to U.S. Provisional Patent Application No. 62/464,058, filed Feb. 27, 2017. The foregoing applications are incorporated by reference herein.

FIELD

[0002] This document relates generally to image processing. More particularly, this document relates to systems and methods for ultrasound image processing facilitating improved cancer diagnosis and treatment monitoring.

BACKGROUND

[0003] Hepatitis C Virus ("HCV") and Non-Alcoholic Fatty Liver Disease ("NAFLD") are the two most common causes of chronic liver disease in North America. It is probably the most common type of liver disease in the United States. In clinical practice, transabdominal ultrasound is most widely used as an initial imaging modality because of its availability, low cost, and no radiation exposure. NAFLD may lead to fibrosis, cirrhosis, liver cancer, liver failure requiring a liver transplant, and mortality. Abdominal ultrasound cannot detect mild hepatic steatosis and cannot differentiate simple steatosis, nonalcoholic steatohepatitis (NASH), and hepatic fibrosis. It is operator dependent, interfered by intra-abdominal gas and technically difficult with poor image quality in obese patients.

SUMMARY

[0004] The present disclosure provides systems and methods for generating enhanced ultrasound images. The ultrasound images processed by the present systems and methods show a soft tissue pattern having a level of visual clarity that enables a medical practitioner to make a liver or kidney disease diagnosis based solely on ultrasound data, without the need of biopsy samples.

[0005] In one aspect, the system may include a non-transitory, computer-readable memory, one or more processors and a computer-readable medium containing programming instructions. The programming instructions, when executed by the one or more processors, cause the system to acquire a raw ultrasound signal output from an ultrasound device and generate filtered ultrasound image data by filtering the raw ultrasound signal to transform information from a signal domain to a frequency domain. The system may also extract image phase and energy features from the filtered ultrasound image data and generate a filtered ultrasound signal by transforming the image phase and energy features from the frequency domain to the signal domain. The system may further produce a transmission map estimation based on a backscattered ultrasound signal from a tissue interface and enhance the image phase and energy features of the filtered ultrasound signal based on the transmission map estimation so that portions of a soft tissue associated therewith are made darker or lighter in an enhanced ultrasound image.

[0006] In some embodiments, the system may perform radial symmetry filtering on the enhanced ultrasound image by analyzing dark spherical shapes in the enhanced ultrasound image and generate a radial symmetry image to identify regions of interest in the enhanced ultrasound image. In some embodiments, the system may additionally output a surface topography map based on the radial symmetry image. In some embodiments, the step of generating the filtered ultrasound image data is performed by a Fourier transform. In some embodiments, the step of generating the filtered ultrasound signal is performed by the inverse Fourier transform.

[0007] In some embodiments, the step of extracting the image phase and energy features is performed by an alpha scale filtering. In some embodiments, the alpha scale filtering is performed in a frequency domain, and the alpha scale filtering can be defined by expression

$$ASF(\omega) = \begin{cases} n_c \omega^a \exp(-(\sigma\omega)^{2\alpha} & \omega > 0 \\ 0 & \text{otherwise} \end{cases}$$

where α is constant derivative parameter, σ is a filter alpha-scale parameter, and n_c is a unit normalization constant calculated from filter α. n_c is computed in accordance with mathematical equation

$$n_c = 2\frac{\sqrt{\pi\alpha}\, 2^{\frac{2a+1}{4\alpha}} s^{a+0.5}}{\sqrt{\Gamma\left(\frac{2a+1}{2\alpha}\right)}}$$

where s is a scale parameter and a is a derivative parameter.

[0008] In some embodiments, the transmission map estimation comprises combining scattering and attenuation effects in soft tissue based on equation

$$US(x,y)=US_A(x,y)US_E(x,y)+(1-US_A(x,y))\alpha$$

where US(x,y) is a local energy image, US_A(x,y) is a signal transmission map, US_E(x,y) is an enhanced ultrasound image, and α is a constant value representative of echogenicity in the soft tissue in a local region. US_E(x,y) can be extracted by estimating the signal transmission map US_A(x, y) using a Beer-Lambert law which models an attenuation function as a function of imaging depth. The Beer-Lambert law is defined by equation

$$US_T(x,y)=US_o(x,y)\exp(-\eta d(x,y))$$

where US_o(x,y) is an initial intensity image, US_T (x,y) is an attenuated intensity image, η is an attenuation coefficient, and d(x,y) is a distance from an ultrasound transducer surface. US_A(x,y) is obtained by minimizing an objective function defined by equation

$$\frac{\lambda}{2}\|US_A(x,y) - US_T(x,y)\|_2^2 + \sum_{j\in\omega}\|W_j o(D_j * US_A(x,y)\|_1$$

where ω is an index set, o represents element wise multiplication, * is a convolution operation, D_j is obtained using a bank of high order differential filters consisting of eight Kirsch filters and one Laplacian filter, and W_j is a weighting matrix calculated in accordance with mathematical equation

$$W_j=\exp(-|D_j(x,y)*US(x,y)|^2)$$

US_E (x,y) is calculated in accordance with equation

$$US_E(x, y) = \left[\frac{US(x, y) - \alpha}{[\max(US_A(x, y), \varepsilon)]^{\phi}}\right] + \alpha.$$

[0009] In some embodiments, the radial symmetry filtering is specified by equation

$$S_n = F_n * A_n$$

where "*" denotes the convolution operation; A_n is an isotropic Gaussian function and F_n is defined as:

$$F_n(p) = \frac{M_n(p)}{k_n}\left(\frac{|\tilde{O}_n((p)|}{k_n}\right)^{\alpha}$$

$$\tilde{O}_n((p) = \begin{cases} O_n(p), O_n(p) < k_n \\ k_n, \text{otherwise} \end{cases}$$

and α is a radial strictness parameter, and k_n is a scaling factor across different radii. The radial symmetry image is defined by equation

$$S = \frac{1}{|N|}\sum_{n \in N} S_n$$

where S is a sum of all symmetry contributions over all ranges considered.

[0010] In another aspect, a method for generating an ultrasound image is also provided. The method includes acquiring, by a computing device, a raw ultrasound signal output from an ultrasound device and generating filtered ultrasound image data by filtering the raw ultrasound signal to transform information from a signal domain to a frequency domain. The method also includes extracting image phase and energy features from the filtered ultrasound image data and generating a filtered ultrasound signal by transforming the image phase and energy features from the frequency domain to the signal domain. The method further includes producing a transmission map estimation based on a backscattered ultrasound signal from a tissue interface and enhancing the image phase and energy features of the filtered ultrasound signal based on the transmission map estimation so that portions of a soft tissue associated therewith are made darker or lighter in an enhanced ultrasound image.

[0011] In some embodiments, the method further includes performing radial symmetry filtering on the enhanced ultrasound image by analyzing dark spherical shapes in the enhanced ultrasound image and generating a radial symmetry image to identify regions of interest in the enhanced ultrasound image. In some embodiments, the method additionally includes outputting a surface topography map based on the radial symmetry image.

DESCRIPTION OF THE DRAWINGS

[0012] The present solution will be described with reference to the following drawing figures, in which like numerals represent like items throughout the figures.

[0013] FIG. **1** shows an example of a process for generating an enhanced ultrasound image.

[0014] FIG. **2** shows an example of a process for generating a radial symmetry image.

[0015] FIG. **3** shows a biopsy (histopathology) image of a non-healthy liver indicating a fatty liver disease.

[0016] FIGS. **4**A-D (collectively "FIG. **4**") show a B-mode (original) ultrasound image of a normal/healthy liver (FIG. **4**A) and an enhanced ultrasound image (FIG. **4**B) of a normal/healthy liver, and a B-mode (original) ultrasound image (FIG. **4**C) of a diseased liver and an enhanced ultrasound image (FIG. **4**D) of a diseased liver.

[0017] FIGS. **5**A-E (collectively "FIG. **5**") show a comparison of different image types; FIG. **5**A shows a B-mode (original) ultrasound image of a normal/healthy liver; FIG. **5**B shows surface topography visualization of a radial symmetry image corresponding to normal/healthy liver tissue; FIG. **5**C shows surface topography visualization of a radial symmetry image corresponding to normal/healthy liver tissue, with different radial symmetry filter parameters applied as compared to FIG. **5**B; and FIG. **5**D shows surface topography visualization of an enhanced ultrasound image corresponding to normal/healthy tissue; FIG. **5**E shows surface topography visualization of an enhanced ultrasound image corresponding to normal/healthy tissue, with different filter parameters used as compared to FIG. **5**D.

[0018] FIGS. **6**A-E (collectively "FIG. **6**") show a comparison of different image types; FIG. **6**A shows a B-mode (original) ultrasound image of a diseased liver; FIG. **6**B shows surface topography visualization of a radial symmetry image corresponding to diseased liver tissue; FIG. **6**C shows surface topography visualization of a radial symmetry image corresponding to diseased liver tissue, with different radial symmetry filter parameters applied as compared to FIG. **6**B; and FIG. **6**D shows surface topography visualization of an enhanced ultrasound image corresponding to diseased tissue; FIG. **6**E shows surface topography visualization of an enhanced ultrasound image corresponding to diseased tissue, with different filter parameters used as compared to FIG. **6**D.

[0019] FIG. **7** is a schematic illustration of an exemplary ultrasound device in which the present solution can be implemented.

[0020] FIG. **8** is a schematic illustration of an exemplary architecture for a computing device.

DETAILED DESCRIPTION

[0021] It will be readily understood that the components of the embodiments as generally described herein and illustrated in the appended figures could be arranged and designed in a wide variety of different configurations. Thus, the following more detailed description of various embodiments, as represented in the figures, is not intended to limit the scope of the present disclosure, but is merely representative of various embodiments. While the various aspects of the embodiments are presented in drawings, the drawings are not necessarily drawn to scale unless specifically indicated.

[0022] The present solution concerns systems and methods for ultrasound image processing and design of a next-generation ultrasound imaging platform in the context of cancer diagnosis and treatment monitoring with a specific focus on kidney and liver. The ultrasound image processing of the present solution uses a raw ultrasound signal to extract

image features from filtered ultrasound data. Previous platforms use image data. These previous platforms suffer from many drawbacks. For example, these previous platforms experience issues due to poor sensitivity and specificity for kidney and liver cancer detection which causes major problems in the management and treatment of cancer. In general, imaging appearances of liver metastases are nonspecific, and biopsy specimens are required for histologic diagnosis. The present solution resolves these drawbacks by implementing a new computational algorithm as described herein in an ultrasound device.

[0023] A biopsy (histopathology) image of a non-healthy liver indicating a fatty liver disease is shown in FIG. **3**. The circular pattern in the biopsy image, as highlighted by arrows, indicates that the liver has a fatty liver disease. However, the circular pattern is not visible or detectable by investigating an ultrasound image. Accordingly, the diagnosis of a disease is complicated based on ultrasound images. There is a need for an image processing device which can enhance the ultrasound data and provide more information useful for making a diagnosis. Such a method is implemented by the present solution.

[0024] In some scenarios, the present solution is used for early detection of fatty liver, liver cancer, and kidney cancer. Biopsies are current the standard technique for such early detection. The present solution does not require obtaining a sample by performing a biopsy. Accordingly, the present solution allows for earlier detection and for detection without unduly stressing the patient.

[0025] The present invention combines different steps in order to create the framework that results in the enhancement of the liver and/or kidney ultrasound data. Optimization of each of the steps is also one of the main contributions. The main part of the algorithm is based on the extraction of local phase image features from liver and kidney ultrasound data. Phase-based image enhancement and processing has been previously proposed to process various medical image data. Image phase information is a key component in the interpretation of a scene that has long been known to contribute more to the visual appearance of an image than magnitude information. Phase features are intensity invariant and more robust to noise which are important characteristics especially for processing ultrasound images. Extraction of phase information is performed in the frequency domain where the B-mode ultrasound image (original image) is transformed to the frequency domain by Fourier transform operation and multiplied with a band-pass quadrature filter.

[0026] Referring now to FIG. **1**, there is provided an illustration of an exemplary method **100** for image enhancement that is useful for understanding the present solution. The combination of the operations of steps **102-108** creates a framework resulting in the enhancement of liver and/or kidney ultrasound data.

[0027] The main part of the process is based on the extraction of local phase image features from an ultrasound signal. Image phase information is a key component in the interpretation of a scene since it contributes more to the visual appearance of an image than magnitude information. Phase features are intensity invariant and more robust to noise which are important characteristics especially for processing ultrasound images.

[0028] Extraction of phase information is performed in the frequency domain where a raw ultrasound signal or a B-mode ultrasound image is received from an ultrasound device as shown by arrow **101**. The raw ultrasound image signal is then transformed from a signal domain to a frequency domain, as shown by **102**. A Fourier transform is used to achieve this transformation. Thereafter, the filtered ultrasound image data is multiplied with a band-pass quadrature filter, as shown by **104**. Fourier transforms, and band-pass quadrature filters are well known in the art. Any known or to be known Fourier transform and/or band-pass quadrature filter can be used herein without limitation. For example, an optimized band-pass quadrature filter is employed in **104**. Optimization is related to selection of filter parameters. Usually, this is performed by trial and error. Once a good set of parameters are found, these are kept constant, and all the ultrasound images are filtered with this optimized filter. However, automatic filter parameter optimization may be employed herein. Techniques for automatic filter parameter optimization is known in the art. Any known or to be known technique for automatic filter parameter optimization can be used herein without limitation.

[0029] In some scenarios, the band-pass quadrature filter comprises an alpha-scale filter. As such, alpha-scale filtering can be employed in **104**. The alpha-scale filtering is performed to extract phase and energy features from a filtered raw ultrasound signal. This feature extraction facilitates the generation of an enhanced ultrasound image showing a soft tissue pattern having a level of visual clarity at which a medical practitioner is able to make a liver or kidney cancer diagnosis exclusively based on ultrasound data. Notably, other frequency domain quadrature filters (e.g., Log Gabor filter) are not suitable for use alone in liver and kidney diagnosis applications because such filtering does not result in enhanced soft tissue features.

[0030] It should be understood that Log Gabor filters are less computationally and resource intensive as compared to alpha-scale filters. Therefore, a person skilled in the art would not be motivated to use alpha-scale filters when processing ultrasound image data. However, the inventors recognized that the combination of alpha-scale filters with the other two Fourier transform process of **102** and transmission map filtering process of **106-108** provides certain non-obvious advantageous when interested in visualizing certain soft tissue features. These advantages include the enhancement of soft tissue features having a level of visual clarity at which a medical practitioner is able to make a liver or kidney cancer diagnosis exclusively based on ultrasound data.

[0031] In some scenarios, an alpha-scale filter in the frequency domain is constructed as defined by the following Equation (1):

$$SF(\omega) = \begin{cases} n_c \omega^{\sigma} \exp(-(\sigma\omega)^{2\alpha}) & \omega \geq 0 \\ 0 & \text{otherwise} \end{cases} \quad (1)$$

where α is constant derivative parameter which is chosen to be α=0.2 in order for the filters to satisfy the DC condition. σ is the filter alpha-scale parameter (for example, in some embodiments, the filter alpha-scale parameter is 25), and n_c is a unit normalization constant calculated from filter α value using the following Equation (2):

$$n_c = 2\frac{\sqrt{\pi\alpha}\,2^{\frac{2a+1}{4\alpha}}\,s^{a+0.5}}{\sqrt{\Gamma\left(\frac{2a+1}{2\alpha}\right)}} \quad (2)$$

where s is a scale parameter and a is a derivative parameter. In some embodiments, the scale parameter is 2, and the derivative parameter is 1.83.

[0032] Filtering the Fourier transformed ultrasound image with the constructed alpha scale filter and using an inverse Fourier transform operation, image phase, and energy features are extracted from the ultrasound image. The local energy image encodes the underlying structural information of the liver or kidney ultrasound image.

[0033] After completing the alpha scale filtering, method **100** continues with **105** where the ultrasound image data is transformed from the frequency domain to the signal domain via an inverse Fourier transform process. The results of **105** are then used in **106** to obtain a transmission map estimation. The interaction of the ultrasound signal within the tissue can be characterized into two main categories (namely, scattering and attenuation). Since the information of the backscattered ultrasound signal (from the tissue interface to the ultrasound transducer) is modulated by these two interactions, they can be viewed as mechanisms of structural information coding. Based on this a model was developed. The model is referred to herein as an ultrasound signal transmission map. The ultrasound signal transmission map is useful for recovering a pertinent liver and/or kidney tissue structure from the ultrasound images. In order to achieve this, a linear interpolation model is employed which combines scattering and attenuation effects in the tissue. The linear interpolation model is defined by the following Equation (3):

$$US(x,y)=US_A(x,y)US_E(x,y)+(1-US_A(x,y))\alpha \quad (3)$$

where US(x,y) is the local energy image calculated in **104**, US_A (x,y) is the signal transmission map, US_E(x,y) is the enhanced liver/kidney ultrasound image, and α is a constant value representative of echogenicity in the tissue in the local region. In the present solution, three different values for α are used to obtain three different enhancement results.

[0034] The local energy image generated in **104** is used in a subsequent filtering process as shown by **106** and **108**. The filtering process of **106** and **108** is generally performed to enhance the extracted phase, and energy features so that portions of the soft tissue associated therewith are made darker or lighter in the enhanced ultrasound image (e.g., as shown in FIG. **3**).

[0035] In **106**, US_E(x,y) is extracted by estimating the signal transmission map US_A(x,y) using a well-known Beer-Lambert law which models the attenuation function as a function of imaging depth. The Beer-Lambert law is defined by the following Equation (4):

$$US_T(x,y)=US_o(x,y)\exp(-\eta d(x,y)) \quad (4)$$

where US_o(x,y) is the initial intensity image (filtered image obtained from the alpha-scale filtering step), US_T(x,y) is the attenuated intensity image, η is the attenuation coefficient (for example, in some embodiments, the attenuation coefficient used is 2), and d(x,y) is the distance from the ultrasound transducer surface.

[0036] Once US_T(x,y) is obtained, US_A(x,y) is obtained by minimizing an objective function defined by Equation (5):

$$\frac{\lambda}{2}\|US_A(x,y)-US_T(x,y)\|_2^2+\sum_{j\in\omega}\|W_j o(D_j * US_A(x,y)\|_1 \quad (5)$$

where ω is an index set, o represents element wise multiplication, and * is a convolution operation. D_j is obtained using a bank of high order differential filters consisting of eight Kirsch filters and one Laplacian filter. W_j is a weighting matrix calculated using the following Equation (6):

$$W_j=\exp(-|D_j(x,y)*US(x,y)|^2) \quad (6)$$

Once US_A(x,y) is estimated, US_E(x,y) is calculated using the following Equation (7):

$$US_E(x,y)=\left[\frac{US(x,y)-\alpha}{[\max(US_A(x,y),\varepsilon)]^\delta}\right]+\alpha \quad (7)$$

[0037] FIG. **3** shows a biopsy (histopathology) image of a non-healthy liver indicating a fatty liver disease. The circular pattern in the biopsy image, as highlighted by arrows, indicates that the liver has a fatty liver disease. However, the circular pattern is not visible or detectable by investigating an ultrasound image (FIGS. **4**A and **4**C). The circular pattern is visible in the enhanced ultrasound images generated through the present solution, as shown in FIG. **4**D generated from a B-mode ultrasound image FIG. **4**C. As such, the present solution provides a method for a medical practitioner to make a liver or kidney disease diagnosis based solely on ultrasound data and circumvent the need to obtain a biopsy specimen.

[0038] Referring now to FIG. **2**, a method for generating radial symmetry image based on the enhanced ultrasound images is provided. The process begins at **201** with by performing radial symmetry filtering the enhanced ultrasound images. The enhanced ultrasound images are further processed by utilizing local radial symmetry to identify the regions of interest in the enhanced images. The analysis relies on the fact that the diseased liver has a higher degree of radial symmetry compared to the healthy liver. The analysis is carried out by searching for dark spherical shapes in the enhanced images using the fast radial feature detection algorithm. At **203**, the process includes generating radial symmetry images, as shown in FIGS. **5**-**6**. FIG. **5**B shows surface topography visualization of radial symmetry image corresponding to normal/healthy liver tissue; FIG. **5**C shows surface topography visualization of radial symmetry image corresponding to normal/healthy liver tissue, with different radial symmetry filter parameters applied as compared to FIG. **5**B. FIG. **6**B shows surface topography visualization of radial symmetry image corresponding to diseased liver tissue; FIG. **6**C shows surface topography visualization of radial symmetry image corresponding to diseased liver tissue, with different radial symmetry filter parameters applied as compared to FIG. **6**B. At **205**, the process optionally includes outputting a surface topography map based on the radial symmetry image. The fast radial symmetry algorithm is described in detail below.

[0039] Fast radial symmetry was used for processing multimedia images. For each radius n, the algorithm uses

image gradients to vote for both the positively and negatively affected pixels. These pixels are calculated using Equations (8) and (9):

$$p_{+ve}(p) = p + \text{round}\left(\frac{g(p)}{\|g(p)\|}n\right) \tag{8}$$

$$p_{-ve}(p) = p - \text{round}\left(\frac{g(p)}{\|g(p)\|}n\right) \tag{9}$$

[0040] In the above equations "round" rounds each vector element to the nearest integer, "g" is the gradient of the image (e.g., the gradient of the enhanced images), "n" represents the radius value for the spherical structures searched in the image. p_{-ve} and p_{+ve} correspond to pixels with gradient g(p) pointing towards and away from the center respectively. Using these pixels and orientation and magnitude projection images, denoted as O_n and M_n respectively, are calculated. For each of the affected pixel, the corresponding point p_{+ve} in O_n and M_n is increased by 1 and ||g(p)|| respectively. Similarly, for the negatively affected pixel, the corresponding point is decreased by the same quantity in each image, as defined by Equations (10)-(13):

$$O_n(p_{+ve}(p)) = O_n(p_{+ve}(p)) + 1 \tag{10}$$

$$O_n(p_{-ve}(p)) = O_n(p_{-ve}(p)) - 1 \tag{11}$$

$$M_n(p_{+ve}(p)) = M_n(p_{+ve}(p)) + \|g(p)\|, \tag{12}$$

$$M_n(p_{-ve}(p)) = M_n(p_{-ve}(p)) - \|g(p)\|, \tag{13}$$

[0041] Using these images, a radial symmetry response image is defined as: $S_n = F_n * A_n$ where "*" denotes the convolution operation. A_n is an isotropic Gaussian function and F_n is defined in Equations (14) and (15):

$$F_n(p) = \frac{M_n(p)}{k_n}\left(\frac{|\tilde{O}_n(p)|}{k_n}\right)^{\alpha} \tag{14}$$

$$\tilde{O}_n(p) = \begin{cases} O_n(p), O_n(p) < k_n \\ k_n, \text{otherwise} \end{cases} \tag{15}$$

[0042] Here α is a radial strictness parameter, and k_n is a scaling factor across different radii. The final full radial symmetry transform is defined by performing this operation for various radii values and summing the resulting feature maps as in Equation (16):

$$S = \frac{1}{|N|}\sum_{n \in N} S_n \tag{16}$$

[0043] The final topography images are obtained by displaying a topography map based on the image intensity values above the radial symmetry and phase images. The diseased liver has a higher topography compared to healthy liver. Examples of surface topography images are shown in FIGS. **5**D-E for a healthy liver and FIGS. **6**D-E for a diseased liver. Specifically, FIG. **5**D shows surface topography visualization of an enhanced ultrasound image corresponding to normal/healthy tissue; FIG. **5**E shows surface topography visualization of an enhanced ultrasound image corresponding to normal/healthy tissue, with different filter parameters used as compared to FIG. **5**D. FIG. **6**D shows surface topography visualization of an enhanced ultrasound image corresponding to diseased tissue; FIG. **6**E shows surface topography visualization of an enhanced ultrasound image corresponding to diseased tissue, with different filter parameters used as compared to FIG. **6**D.

[0044] Referring now to FIG. **7**, there is provided a schematic illustration of an exemplary ultrasound device **700** in which the present solution can be implemented. The ultrasound device **700** comprises a device stand **702** in which a computing device **704** is disposed. Computing device **704** is generally configured to control the operations of the ultrasound device **700**. Such control can be in response to user-software interactions via an input device **716** and/or in accordance with pre-defined rules. A robotic arm **706** is movably attached to the device stand **702**. The robotic arm **706** includes, but is not limited to, an articulating arm with a plurality of joints **708**. An ultrasound transducer **710** is disposed at a distal end of the robotic arm **706**. The ultrasound transducer **710** is moved over an object's surface **712** to be examined and generates a raw ultrasound signal. The object is arranged on a patient positioning table **714**. The raw ultrasound signal is provided to the local computing device **704** or a remote computing device for processing in accordance with the present solution. The results of this processing is a transformation of the raw ultrasound data into an enhanced ultrasound image (e.g., such as that shown in FIG. **4**).

[0045] Referring now to FIG. **8**, there is provided an illustration of an exemplary architecture for a computing device **800**. Computing device **800** may be local to an ultrasound device (e.g., the ultrasound device **700** of FIG. **7**). In this case, computing device **704** is the same as or substantially similar to computing device **800**. In other scenarios, the computing device **800** is located remote from the ultrasound device. In this case, the computing device **704** of the ultrasound device includes a network interface that facilitates communication between the two computing devices over a network (e.g., the Intranet or Internet).

[0046] Computing device **800** may include more or fewer components than those shown in FIG. **8**. However, the components shown are sufficient to disclose an illustrative embodiment implementing the present solution. The hardware architecture of FIG. **8** represents one embodiment of a representative computing device configured to facilitate the generation of an enhanced ultrasound image based on a raw ultrasound signal. As such, the computing device **800** of FIG. **8** implements at least a portion of a method for providing such an enhanced ultrasound image in accordance with the present solution.

[0047] Some or all the components of the computing device **800** can be implemented as hardware, software and/or a combination of hardware and software. The hardware includes, but is not limited to, one or more electronic circuits. The electronic circuits can include, but are not limited to, passive components (e.g., resistors and capacitors) and/or active components (e.g., amplifiers and/or microprocessors). The passive and/or active components can be adapted to, arranged to and/or programmed to perform one or more of the methodologies, procedures, or functions described herein.

[0048] As shown in FIG. **8**, the computing device **800** comprises a user interface **802**, a Central Processing Unit

("CPU") **806**, a system bus **810**, a memory **812** connected to and accessible by other portions of computing device **800** through the system bus **810**, and hardware entities **814** connected to system bus **810**. The user interface can include input devices (e.g., a keypad **850**, a cursor control device **858**, and/or a camera **860**) and output devices (e.g., speaker **852**, a display **854**, and/or light emitting diodes **856**), which facilitate user-software interactions for controlling operations of the computing device **800**.

[0049] At least some of the hardware entities **814** perform actions involving access to and use of memory **812**, which can be a Random Access Memory ("RAM"), a disk driver and/or a Compact Disc Read Only Memory ("CD-ROM"). Hardware entities **814** can include a disk drive unit **816** comprising a computer-readable storage medium **818** on which is stored one or more sets of instructions **820** (e.g., software code) configured to implement one or more of the methodologies, procedures, or functions described herein. The instructions **820** can also reside, completely or at least partially, within the memory **812** and/or within the CPU **806** during execution thereof by the computing device **800**. The memory **812** and the CPU **806** also can constitute machine-readable media. The term "machine-readable media," as used here, refers to a single medium or multiple media (e.g., a centralized or distributed database, and/or associated caches and RPUs) that store the one or more sets of instructions **820**. The term "machine-readable media," as used here, also refers to any medium that is capable of storing, encoding or carrying a set of instructions **820** for execution by the computing device **800** and that cause the computing device **800** to perform any one or more of the methodologies of the present disclosure.

[0050] In some scenarios, the hardware entities **814** include an electronic circuit (e.g., a processor) programmed for facilitating the provision of an enhanced ultrasound image. In this regard, it should be understood that the electronic circuit can access and run a software application **864** installed on the computing device **800**. The software application **824** is generally operative to facilitate the generation of the enhanced ultrasound image. Other functions of the software application **864** will become apparent as the discussion progresses.

[0051] The software application **864** implementing the present solution described herein is stored as a software program in a computer-readable storage medium and is configured for running on the CPU **806**. Furthermore, software implementations of the present solution can include, but are not limited to, distributed processing, component/object distributed processing, parallel processing, virtual machine processing. In the various scenarios, a network interface device **862** connected to a network environment communicates over the network using the instructions **820**.

[0052] The present solution may be embodied in other specific forms without departing from its spirit or essential characteristics. The described embodiments are to be considered in all respects only as illustrative and not restrictive. The scope of the invention is, therefore, indicated by the appended claims rather than by this detailed description. All changes which come within the meaning and range of equivalency of the claims are to be embraced within their scope.

[0053] Reference throughout this specification to features, advantages, or similar language does not imply that all of the features and advantages that may be realized with the present invention should be or are in any single embodiment of the invention. Rather, language referring to the features and advantages is understood to mean that a specific feature, advantage, or characteristic described in connection with an embodiment is included in at least one embodiment of the present invention. Thus, discussions of the features and advantages, and similar language, throughout the specification may, but do not necessarily, refer to the same embodiment.

[0054] Furthermore, the described features, advantages and characteristics of the invention may be combined in any suitable manner in one or more embodiments. One skilled in the relevant art will recognize, in light of the description herein, that the invention can be practiced without one or more of the specific features or advantages of a particular embodiment. In other instances, additional features and advantages may be recognized in certain embodiments that may not be present in all embodiments of the invention.

[0055] Reference throughout this specification to "one embodiment," "an embodiment," or similar language means that a particular feature, structure, or characteristic described in connection with the indicated embodiment is included in at least one embodiment of the present invention. Thus, the phrases "in one embodiment," "in an embodiment," and similar language throughout this specification may, but do not necessarily, all refer to the same embodiment.

[0056] As used in this document, the singular form "a," "an," and "the" include plural references unless the context clearly dictates otherwise. Unless defined otherwise, all technical and scientific terms used herein have the same meanings as commonly understood by one of ordinary skill in the art. As used in this document, the term "comprising" means "including, but not limited to."

[0057] All of the apparatus, methods, and algorithms disclosed and claimed herein can be made and executed without undue experimentation in light of the present disclosure. While the invention has been described in terms of preferred embodiments, it will be apparent to those having ordinary skill in the art that variations may be applied to the apparatus, methods, and sequence of steps of the method without departing from the concept, spirit, and scope of the invention. More specifically, it will be apparent that certain components may be added to, combined with, or substituted for the components described herein while the same or similar results would be achieved. All such similar substitutes and modifications apparent to those having ordinary skill in the art are deemed to be within the spirit, scope, and concept of the invention as defined.

[0058] The features and functions disclosed above, as well as alternatives, may be combined into many other different systems or applications. Various presently unforeseen or unanticipated alternatives, modifications, variations or improvements may be made by those skilled in the art, each of which is also intended to be encompassed by the disclosed embodiments.

What is claimed is:

1. A system for generating an ultrasound image, comprising:

a non-transitory, computer readable memory;

one or more processors; and

a computer-readable medium containing programming instructions that, when executed by the one or more processors, cause the system to:

acquire a raw ultrasound signal output from an ultrasound device;

generate filtered ultrasound image data by filtering the raw ultrasound signal to transform information from a signal domain to a frequency domain;

extract image phase and energy features from the filtered ultrasound image data;

generate a filtered ultrasound signal by transforming the image phase and energy features from the frequency domain to the signal domain;

produce a transmission map estimation based on a back-scattered ultrasound signal from a tissue interface; and

enhance the image phase and energy features of the filtered ultrasound signal based on the transmission map estimation so that portions of a soft tissue associated therewith are made darker or lighter in an enhanced ultrasound image.

2. The system of claim **1**, further comprising programming instructions, when executed by the one or more processors, causing the system to

perform radial symmetry filtering on the enhanced ultrasound image by analyzing dark spherical shapes in the enhanced ultrasound image; and

generate a radial symmetry image to identify regions of interest in the enhanced ultrasound image.

3. The system of claim **2**, further comprising programming instructions, when executed by the one or more processors, causing the system to output a surface topography map based on the radial symmetry image.

4. The system of claim **1**, wherein the step of extracting the image phase and energy features is performed by an alpha scale filtering.

5. The system of claim **4**, wherein the alpha scale filtering is performed in a frequency domain.

6. The system of claim **5**, wherein the alpha scale filtering is defined by expression

$$ASF(\omega)=\begin{cases} n_c\omega^{\alpha}\exp(-(\sigma\omega)^{2\alpha}) & \omega>0 \\ 0 & \text{otherwise} \end{cases}$$

where α is constant derivative parameter, σ is a filter alpha-scale parameter, and n_c is a unit normalization constant calculated from filter α.

7. The system of claim **6**, wherein n_c is computed in accordance with mathematical equation

$$n_c=2\frac{\sqrt{\pi\alpha}\,2^{\frac{2a+1}{4\alpha}}s^{a+0.5}}{\sqrt{\Gamma\left(\frac{2a+1}{2\alpha}\right)}}$$

where s is a scale parameter and a is a derivative parameter.

8. The system of claim **1**, wherein the transmission map estimation comprises combining scattering and attenuation effects in soft tissue based on equation

$$US(x,y)=US_A(x,y)US_E(x,y)+(1-US_A(x,y))\alpha$$

where US(x,y) is a local energy image, US_A(x,y) is a signal transmission map, US_E(x,y) is an enhanced ultrasound image, and α is a constant value representative of echogenicity in the soft tissue in a local region.

9. The system of claim **8**, wherein US_E(x,y) is extracted by estimating the signal transmission map US_A(x,y) using a Beer-Lambert law which models an attenuation function as a function of imaging depth.

10. The system of claim **9**, wherein the Beer-Lambert law is defined by equation

$$US_T(x,y)=US_o(x,y)\exp(-\eta d(x,y))$$

where US_o(x,y) is an initial intensity image, US_T(x,y) is an attenuated intensity image, η is an attenuation coefficient, and d(x,y) is a distance from an ultrasound transducer surface.

11. The system of claim **10**, wherein US_A(x,y) is obtained by minimizing an objective function defined by equation

$$\frac{\lambda}{2}\|US_A(x,y)-US_T(x,y)\|_2^2+\sum_{j\in\omega}\|W_j o(D_j * US_A(x,y)\|_1$$

where ω is an index set, o represents element wise multiplication, * is a convolution operation, D_j is obtained using a bank of high order differential filters consisting of eight Kirsch filters and one Laplacian filter, and W_j is a weighting matrix calculated in accordance with mathematical equation

$$W_j=\exp(-|D_j(x,y)*US(x,y)|^2)$$

12. The system of claim **11**, wherein US_E(x,y) is calculated in accordance with equation

$$US_E(x,y)=\left[\frac{US(x,y)-\alpha}{[\max(US_A(x,y),\varepsilon)]^{\delta}}\right]+\alpha.$$

13. The system of claim **2**, wherein the radial symmetry filtering is specified by equation

$$S_n=F_n*A_n$$

where "*" denotes the convolution operation; A_n is an isotropic Gaussian function and F_n is defined as:

$$F_n(p)=\frac{M_n(p)}{k_n}\left(\frac{|\widetilde{\mathcal{O}}_n(p)|}{k_n}\right)\alpha$$

$$\widetilde{\mathcal{O}}_n(p)=\begin{cases} O_n(p), & O_n(p)<k_n \\ k_n, & \text{otherwise} \end{cases}$$

and α is a radial strictness parameter, and k_n is a scaling factor across different radii.

14. The system of claim **2**, wherein the radial symmetry image is defined by equation

$$S=\frac{1}{|N|}\sum_{n\in N}S_n$$

where S is a sum of all symmetry contributions over all ranges considered.

15. A method for generating an ultrasound image, comprising:

acquiring, by a computing device, a raw ultrasound signal output from an ultrasound device;

generating filtered ultrasound image data by filtering the raw ultrasound signal to transform information from a signal domain to a frequency domain;

extracting image phase and energy features from the filtered ultrasound image data;

generating a filtered ultrasound signal by transforming the image phase and energy features from the frequency domain to the signal domain;

producing a transmission map estimation based on a backscattered ultrasound signal from a tissue interface; and

enhancing the image phase and energy features of the filtered ultrasound signal based on the transmission map estimation so that portions of a soft tissue associated therewith are made darker or lighter in an enhanced ultrasound image.

16. The method of claim **15**, further comprising:

performing, by a computing device, radial symmetry filtering on the enhanced ultrasound image by analyzing dark spherical shapes in the enhanced ultrasound image; and

generating, by a computing device, a radial symmetry image to identify regions of interest in the enhanced ultrasound image.

17. The method of claim **16**, further comprising outputting a surface topography map based on the radial symmetry image.

18. The method of claim **15**, wherein the backscattered ultrasound signal is modulated by interactions with a tissue, the interactions comprising scattering and attenuation.

19. The method of claim **15**, wherein the step of generating the filtered ultrasound image data is performed by a Fourier transform.

20. The method of claim **15**, wherein the step of generating the filtered ultrasound signal is performed by the inverse Fourier transform.

21.-**31**. (canceled)

* * * * *

专利名称(译)	计算超声改善肝脏和肾脏癌的诊断		
公开(公告)号	US20200065948A1	公开(公告)日	2020-02-27
申请号	US16/489151	申请日	2018-02-27
申请(专利权)人(译)	罗格斯新泽西州立大学		
当前申请(专利权)人(译)	罗格斯新泽西州立大学		
[标]发明人	NOSHER JOHN HACIHALILOGLU ILKER		
发明人	NOSHER, JOHN HACIHALILOGLU, ILKER		
IPC分类号	G06T5/00 G06T5/10 G06T5/20 A61B8/08		
CPC分类号	G06T2207/30056 A61B8/5207 G06T5/10 G06T5/20 G06T5/008 G06T2207/10132 G06K9/4609 G06T5/003		
优先权	62/464058 2017-02-27 US		
外部链接	Espacenet USPTO		

摘要(译)

本公开提供了一种用于产生超声图像的系统和方法。 该方法包括接收从超声设备输出的原始超声信号，并执行将原始超声信号转换成增强的超声图像的操作。 增强的超声图像可以通过径向对称滤波被进一步处理以生成径向对称图像。 增强图像和径向对称图像都可以由医学从业人员仅基于超声数据进行肝癌或肾癌诊断。

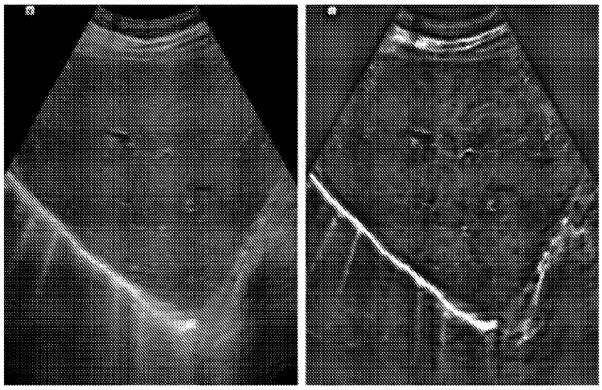

Normal/Healthy Liver

Enhanced Normal/Healthy Liver